

CHANDRA OBSERVATIONS OF THE THREE MOST METAL-DEFICIENT BLUE COMPACT DWARF GALAXIES KNOWN IN THE LOCAL UNIVERSE, SBS 0335–052, SBS 0335–052W, AND I ZW 18

TRINH X. THUAN,¹ FRANZ E. BAUER,² POLICHRONIS PAPADEROS,³ AND YURI I. IZOTOV⁴

(Received 10 November 2003; Accepted 16 January 2004)

The Astrophysical Journal, Accepted

ABSTRACT

We present an X-ray study of the three most metal-deficient blue compact dwarf (BCD) galaxies known in the local Universe, based on deep *Chandra* observations of SBS 0335–052 (0.025Z_⊙), SBS 0335–052W (0.02Z_⊙) and I Zw 18 (0.02Z_⊙). All three are detected, with more than 90% of their X-ray emission arising from point-like sources. The 0.5–10.0 keV luminosities of these point sources are in the range $(1.3\text{--}8.5)\times 10^{39}$ erg s⁻¹. We interpret them to be single or a collection of high-mass X-ray binaries, the luminosities of which may have been enhanced by the low metallicity of the gas. There are hints of faint extended diffuse X-ray emission in both SBS 0335–052 and I Zw 18, probably associated with the superbubbles visible in both BCDs. The spectrum of I Zw 18 shows a O VIII hydrogen-like emission line. The best spectral fit gives an O overabundance of the gas in the X-ray point source by a factor of ~ 7 with respect to the Sun, or a factor of ~ 350 with respect to the O abundance determined for the HII region.

Subject headings: galaxies: individual: I Zw 18 — galaxies: individual: SBS 0335–052 — galaxies: individual: SBS 0335–052W — galaxies: starburst — X-rays: galaxies

1. INTRODUCTION

Galaxy formation is one of the most fundamental problems in astrophysics. To understand how galaxies form, we need to unravel how stars form from the primordial gas and how the first stars interact with their surrounding environments. As there are no heavy elements in the early universe, the thermodynamic behavior of the gas is essentially controlled by H₂ cooling, and the first Population III stars are expected to be very massive (e.g., Abel, Bryan, & Norman 2002; Bromm, Coppi, & Larson 2002). While much progress has been made in finding large populations of galaxies at high ($z \geq 3$) redshifts (e.g., Steidel et al. 1996), truly young galaxies in the process of forming remain elusive in the distant universe. The spectra of those far-away galaxies generally indicate the presence of a substantial amount of heavy elements, implying previous star formation and metal enrichment. Instead of focussing on high-redshift galaxies, another approach is to study massive star formation and its interaction with the ambient interstellar medium (ISM) in a class of nearby metal-deficient dwarf galaxies called Blue Compact Dwarf (BCD) galaxies, some of which are thought to be undergoing their first episode of star formation.

The formation of the hot gas phase is one of the most fundamental processes operating in the early period of galaxy formation and it has important consequences on the subsequent dynamical state and photometric evolution of the dwarf system. The generation of large amounts of hot (a few $\times 10^6$ K), rarefied gas is the result of injection of energy and momentum into the cold ambient ISM by stellar winds from massive stars and supernovae. The starburst activity which fuels the ISM of young dwarf galaxies with hot X-ray emitting gas lasts about

10 million years. It is then followed by a long ($> 1\text{--}2$ Gyr) quiescent period of passive photometric evolution. Moreover, expansion of the hot ISM on scales comparable to the galactic scale length can lead to a rapid funneling of gaseous mass into the cold gaseous halo. The details of such a process are expected to be sensitively related to the energy injection rate into the ISM and the geometry and robustness of the ambient cold gaseous medium (De Young & Heckman 1994). Extensive mass loss can lead to an expansion of the stellar population and to a morphological evolution of the dwarf galaxy (for example a dwarf irregular galaxy may lose its gas and evolve into a dwarf elliptical) or even disrupt the system entirely (Hills 1980; Yoshii & Arimoto 1987).

Here we present a study at X-ray energies of the three most metal-deficient star-forming dwarf galaxies known in the local universe, the BCDs SBS 0335–052 (Thuan & Izotov 1997; Izotov et al. 1997; Thuan, Izotov, & Lipovetsky 1997, hereafter TIL), SBS 0335–052W (Lipovetsky et al. 1999), and I Zw 18 (see Papaderos et al. 2002, Hunt, Thuan, & Izotov 2003a, and references therein). X-ray emission provides an efficient and direct probe of the hot gas component, and can provide valuable constraints on the nature of the X-ray binary population. The number of high mass X-ray binaries (HMXBs) put limits on the BCD's supernova rate while the number of low mass X-ray binaries (LMXBs) constrains the total mass of forming stars. The relative proximity of these three BCDs [$D = 54.3$ Mpc for SBS 0335–052 and SBS 0335–052W (TIL); $D = 12.6$ Mpc for I Zw 18 (Östlin 2000)], their extremely low metallicities [0.025Z_⊙ for SBS 0335–052 (Izotov et al. 1999), 0.020Z_⊙ for SBS 0335–052W (Lipovetsky et al. 1999), and 0.020Z_⊙ for I Zw 18 (Izotov et al. 1999)], and high neutral gas content (see Pustilnik et al. 2001 for SBS 0335–052 and SBS 0335–052W and van Zee et al. 1998 for I Zw 18) make them the best local approximations to primordial young galaxies. Their relatively bright apparent magnitudes ($m_B = 17.0$ mag for SBS 0335–052, $m_B = 19.4$ mag for SBS 0335–052W and $m_B = 15.8$ mag for I Zw 18) make them much easier to study than the very faint and small

¹ Astronomy Department, University of Virginia, P.O. Box 3818, University Station, Charlottesville, VA, 22903, USA; txt@virginia.edu

² Institute of Astronomy, University of Cambridge, Madingley Rd., Cambridge, CB3 0HA, UK; feb@ast.cam.ac.uk

³ Universitäts-Sternwarte, Geismarlandstrasse 11, D-37083 Göttingen, Germany; papade@uni-sw.gwdg.de

⁴ Main Astronomical Observatory, National Academy of Sciences of Ukraine, 03680 Kyiv, Ukraine; izotov@mao.kiev.ua

building-block dwarf galaxies at high-redshift. HI VLA mapping (Pustilnik et al. 2001) shows SBS 0335–052 and SBS 0335–052W to be embedded in a common very large HI envelope with an overall size of $\sim 66 \times 22$ kpc. There are two prominent HI peaks separated in the east-west direction by 22 kpc ($84''$). The eastern peak is associated with SBS 0335–052, while the western peak is about a factor of 1.3 brighter in the HI line and is associated with the fainter SBS 0335–052W. Likewise, HI VLA mapping of I Zw 18 by van Zee et al. (1998) shows that it is also embedded in an extended HI envelope.

Optical *HST* imaging shows that nearly all star formation in SBS 0335–052 occurs in six very blue super-star clusters (SSCs) with absolute V luminosities between -11.7 and -14.7 mag, and surface brightnesses $\gtrsim 100$ times those of clusters and associations in normal HII regions. The SSCs are confined to a region of about 520 pc in diameter (TIL). There is a systematic color gradient from the brightest and bluest SSC at one end to the faintest and reddest SSC at the other end. Such behavior can be attributed partly to variable dust extinction. Dust is clearly present, even in such a metal-poor environment, as evidenced by the strong mid-infrared emission of SBS 0335–052 (Thuan, Savage, & Madden 1999). However, most of the color gradient is due to a systematic aging of the SSCs resulting from sequential propagating star formation (with a velocity ≤ 20 km s $^{-1}$) from the reddest and oldest SSC to the bluest and youngest one (Papaderos et al. 1998). From the $V-I$ colors and the models of Leitherer & Heckman (1995), the age of the youngest SSC is ~ 4 Myr while that of the oldest SSC is ~ 30 Myr. On larger scales, the light of SBS 0335–052 is dominated by a patchy and filamentary very blue low surface brightness (LSB) emission. Spectroscopic studies (Izotov et al. 1997) have revealed that ionized gas contributes $\sim 30\%$ of the emission from the LSB component, out to scales of ~ 3 kpc. The remaining $\sim 70\%$ of the light comes from an underlying stellar population which Papaderos et al. (1998) have shown is not older than ~ 500 Myr. A striking signature of the collective action of massive stars and SNe on the ISM of SBS 0335–052 is a large supershell with radius ~ 380 pc to the North of the SSCs. TIL estimate the star formation rate in SBS 0335–052 from its $H\alpha$ luminosity to be $\sim 0.4 M_{\odot} \text{ yr}^{-1}$.

SBS 0335–052W has been studied in detail by Lipovetsky et al. (1999). It has the same redshift as SBS 0335–052 and consists of at least three stellar clusters. It has also a very low metallicity of $\sim 2\%$ solar and is about 2.4 magnitudes fainter than SBS 0335–052. Its very blue $R-I$ colors also suggest a very young age of less than ~ 500 Myr.

I Zw 18 is composed of two bright knots of star formation separated by $5''$ and referred to as the brighter northwest (NW) and fainter southeast (SE) components (Papaderos et al. 2002). Star formation proceeds differently in I Zw 18 as compared to SBS 0335–052. There are no SSCs in I Zw 18 and the derived SFR is one order of magnitude smaller ($\sim 0.04 M_{\odot} \text{ yr}^{-1}$) than in SBS 0335–052. Papaderos et al. (2002) and Hunt, Thuan, & Izotov (2003a), using deep optical and near-infrared imaging, have put an upper limit of ~ 500 Myr for the age of I Zw 18.

In §2 we describe the properties of the X-ray sources and their optical properties. In §3 we summarize our findings and discuss the X-ray properties of SBS 0335–052 and I Zw 18 in the broader context of star formation in a low-metallicity environment.

2. OBSERVATIONS AND DATA REDUCTION

2.1. X-ray Observations

SBS 0335–052 was observed on 2000 September 7 with ACIS-I (the imaging array of the Advanced CCD Imaging Spectrometer; Garmire et al. 2002) aboard the *Chandra* satellite. The field of view of $16'9 \times 16'9$ was large enough to include also SBS 0335–052W. Events were telemetered in Very Faint mode, and the CCD temperature was -120° C. To compare the X-ray properties of SBS 0335–052 with those of another extremely metal-deficient BCD, we have retrieved from the *Chandra* archive the data for the BCD I Zw 18. This galaxy was observed on 2000 February 8 (P.I: D.J. Bomans) with ACIS-S (chips 235678 on, $8'5 \times 8'5$ per chip). Events were telemetered in Faint mode, and the CCD temperature was -120° C. The ACIS pixel size is $0''.492$ while the half-energy radius of an on-axis point source is $\approx 0''.42$.

Analysis was done using primarily the CIAO V2.3 software provided by the *Chandra* X-ray Center (CXC), but also with FTOOLS and custom software. We removed the $0''.5$ pixel randomization, cleaned the ACIS background using Very Faint mode screening for SBS 0335–052, performed standard ASCA grade selection, and excluded bad pixels and columns. The total net exposure times were 61,042 s for SBS 0335–052 and 40,776 s for I Zw 18. The average quiescent background rates for SBS 0335–052 and I Zw 18 were found to be 0.3 and 0.96 counts s $^{-1}$ per chip, respectively, in good agreement with ACIS-I and ACIS-S calibration measurements. The observation of SBS 0335–052 contained four background “flares”, the intensity of each being about three times the quiescent level and lasting for 5–10% of the total exposure. The observation of I Zw 18 contained one flare about ten times the quiescent level lasting for 20% of the total exposure⁵. None of the flares were strong enough to warrant removal. The resulting average background level is thus ≈ 0.02 counts pixel $^{-1}$ and ≈ 0.06 counts pixel $^{-1}$, respectively.

2.2. Astrometry of optical and X-ray images

To compare the X-ray emission with the optical emission, we have overlaid the X-ray contours over the V -band (F569W) *HST* WFPC2 image of SBS 0335–052 obtained by TIL and the V -band (F555W) *HST* WFPC2 image of I Zw 18 retrieved from the archives and reprocessed by Papaderos et al. (2002). As SBS 0335–052W does not lie within the field of view of any *HST* image, we have used for optical comparison the CCD B -band image obtained by Papaderos et al. (1998) with the 2.2 m Calar Alto telescope. The Calar Alto image has a large field of view ($\sim 17' \times 17'$), and contains enough stars for aligning the *HST* and X-ray images to the same astrometric reference frame. A similar alignment was performed for I Zw 18 using the CCD B -band image obtained by Papaderos et al. (2002), also with the 2.2 m Calar Alto telescope. To align the optical images, sources were first extracted from the Calar Alto images using SExtractor (v2.2.1; Bertin & Arnouts 1996). Optical sources from the Calar Alto images were matched to the GSC2.2 catalog for absolute astrometric alignment, giving a coincidence of 28 sources within a 3σ radius of $0''.57$ and a rms scatter of $0''.25$ for SBS 0335–052, and 25 sources within a 3σ radius of $0''.62$ and a rms scatter of $0''.23$ for I Zw 18. In the same manner, optical sources from the Calar Alto image were used to align the *HST* images (TIL; Papaderos et al. 2002) to the same ref-

⁵ See <http://cxc.harvard.edu/contrib/maxim/bg/index.html>

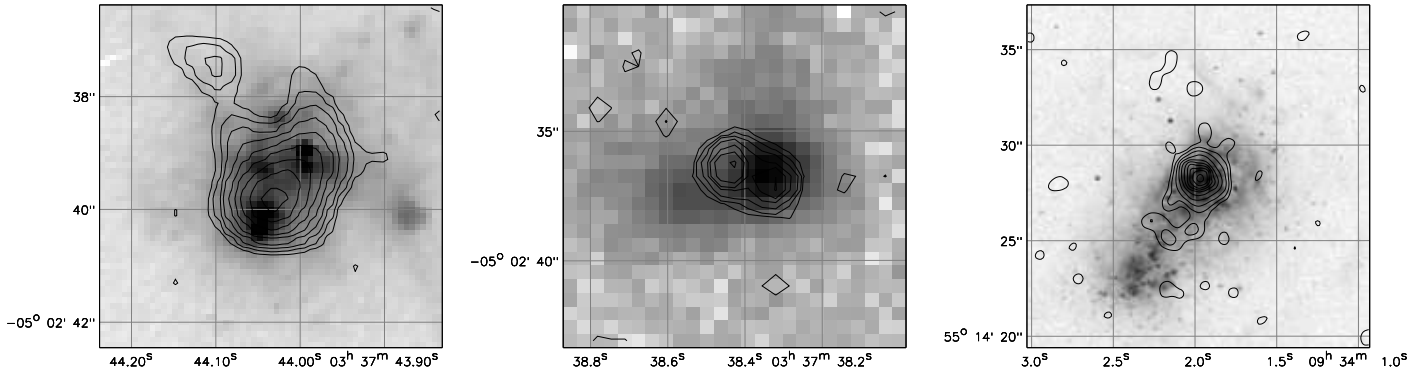


FIG. 1.— X-ray contours overlaid on a *HST* WFPC2 F569W image (TIL) of SBS 0335–052 (left), a *B*-band Calar Alto image (Papaderos et al. 1998) of SBS 0335–052W (middle) and a *HST* WFPC2 F555W image (Papaderos et al. 2002) of I Zw 18 (right).

erence frame; 51 sources were matched within a $0''.82$ radius and a rms scatter of $0''.31$ for SBS 0335–052, while 21 sources were matched within a $0''.49$ radius and a rms scatter of $0''.19$ for I Zw 18.

To align the Chandra image, we first extracted the X-ray sources using the CIAO wavelet algorithm WAVDETECT on the 0.5–8.0 keV images with a probability threshold of 10^{-7} (Freeman et al. 2002), which is equivalent to the detection of approximately one false source over the entire ACIS array. Eighty sources were detected in total in the SBS 0335–052 field. Positions and counts for the sources were determined using fixed circular apertures with 95% encircled energy radii (based on point spread functions (PSF) derived from MKPSF and the PSF library). Sixty-four sources lie within the region imaged by Papaderos et al. (1998) around SBS 0335–052, of which 18 X-ray sources have plausible optical counterparts within a 3σ radius of $0''.9$, including both SBS 0335–052 and SBS 0335–052W. Less than 2 false matches are expected. Aligning the X-ray image to the optical astrometric reference frame based on these SBS 0335–052 X-ray/optical matches, we find that the astrometric accuracy of the X-ray positions has a rms scatter of $0''.42$. Likewise, 16 sources lie within the region imaged by Papaderos et al. (2002) around I Zw 18, but only four X-ray sources have plausible optical counterparts within a 3σ radius of $1''.7$, including I Zw 18. This paucity of matches is likely due to the relatively shallow depth of the *B*-band Calar Alto image. Less than 1 false match is expected. Aligning the X-ray image to the optical astrometric reference frame based on these I Zw 18 X-ray/optical matches, we find that the astrometric accuracy of the X-ray positions has a rms scatter of $0''.55$.

2.3. X-ray Analysis

Based on our astrometric solutions, we present X-ray contours of SBS 0335–052, SBS 0335–052W, and I Zw 18 in Figure 1, overlaid on optical images. SBS 0335–052 consists of a faint X-ray point source (29 counts) lying $\approx 0''.3$ north of SSC 2. We follow here the SSC numbering scheme of TIL. Because the X-ray position is no more accurate than $0''.42$, the data is consistent with the X-ray source being physically associated with SSC 2. The elongated shapes of the faint X-ray contours to the north suggest that there may also be X-ray emission associated with SSC 3 and the pair of SSC 4 and 5. There is also a very faint X-ray source to the northeast which appears to be associated with the supernova cavity seen in the optical image (TIL). Excluding the source near SSC 2, the

total X-ray emission of the fainter features is $\lesssim 23$ counts (Table 1), making it virtually impossible to distinguish between point-like and truly extended emission.

Although SBS 0335–052W is 2.4 mag fainter in *B* than SBS 0335–052, it is 2.8 times brighter in the X-ray. It consists of two faint X-ray point sources. The fainter one appears to be spatially coincident with the brightest of the two optical clusters in SBS 0335–052W. The brighter X-ray source lies $\approx 1''.8$ to the northeast and does not appear to have an optical counterpart.

I Zw 18 is only 1.2 mag brighter in *B* than SBS 0335–052, but its X-ray flux is more than 10 times higher than that of SBS 0335–052. It consists of a single X-ray point source (471 counts) and a very faint extended X-ray component (22 counts). The point source is spatially coincident with the bright NW component of I Zw 18. The faint extended component appears to lie along the main body of I Zw 18 with some X-ray emission centered on the northwest component and some in between the northwest and southeast optical peaks. Bomans & Weis (2002) in a preliminary reduction of the same Chandra data also found the X-ray emission of I Zw 18 to be composed of a strong point source and fainter extended emission, although we fail to recover the SW and NE extensions these authors claim to see.

X-ray variability is an extremely useful method for constraining the size of the emitting region. Because *Chandra* records the position, energy, and time of all incoming photons, we can use this information to search for short-term variability over the duration of our observation. We searched for variability from the different X-ray components of SBS 0335–052, SBS 0335–052W, and I Zw 18 using the Kolmogorov-Smirnov (KS) test. While no significant variability was found, the limited statistics do not strongly constrain the temporal nature of the sources.

X-ray spectra can provide information about the mechanisms by which the X-ray emission is generated. The X-ray spectra were analyzed using XSPEC (v11.2 Arnaud 1996). Unless stated otherwise, spectral parameter errors are for the 90% confidence level, assuming one parameter of interest. The X-ray fluxes and absorption-corrected luminosities for all sources were calculated from spectral fitting using XSPEC. Importantly, none of the sources of interest suffer from pileup.

To constrain the fit of the X-ray spectra, it is important to use accurate HI column densities for each of the objects. The HI column density towards SBS 0335–052 has been derived by (Thuan & Izotov 1997) through fitting the wings of

TABLE 1. X-RAY EMISSION FROM SBS 0335–052, SBS 0335–052W, AND I Zw 18

(1) Source	(2) Position	(3) Counts	(4) Model	(5) N_{H}	(6) Γ/kT	(7) Fit/DOF	(8) F_{X}	(9) L_{X}	(10) Comments
SBS 0335–052	033744.1-050239.5	29.3 ± 6.5	POW	$6.8 (< 16.3)$	$2.1^{+1.5}_{-1.2}$	24.8/24	6.1	3.5	Point Src.
			RAY	$5.9^{+6.3}_{-5.4}$	$3.6 (> 1.2)$	24.7/24	5.2	2.8	
			POW	7.0 (fixed)	$2.2^{+0.6}_{-0.8}$	24.8/25	5.7	3.5	
			RAY	7.0 (fixed)	$2.7^{+16.6}_{-1.3}$	24.6/25	4.5	2.8	
			RAY	7.0 (fixed)	1.0 (fixed)		0.6	0.64	
SBS 0335–052W	033738.5-050236.5	82.4 ± 10.2	POW	$5.2^{+3.3}_{-2.7}$	$2.8^{+0.9}_{-0.8}$	41.1/56	10.3	8.5	Point Src. #1
			RAY	$3.1^{+2.7}_{-1.9}$	$2.0^{+2.2}_{-1.8}$	41.6/56	9.6	5.2	
	033738.4-050237.3	36.4 ± 7.1	POW	$2.3 (< 7.1)$	$1.9^{+1.1}_{-0.8}$	21.9/30	6.3	2.8	Point Src. #2
			RAY	$1.3 (< 3.0)$	$5.4 (> 1.9)$	22.0/30	5.9	2.4	
I Zw 18	093401.9+551428.4A	469.5 ± 21.7	POW	$1.44^{+0.38}_{-0.37}$	$2.01^{+0.14}_{-0.16}$	18.1/20*	72.1	1.6	Point Src., 0.65 keV line?
			RAY	$0.87^{+0.27}_{-0.24}$	$4.06^{+1.84}_{-1.19}$	23.0/20*	66.6	1.4	
			VRAY	$0.94^{+0.35}_{-0.24}$	$4.28^{+2.25}_{-1.31}$	8.1/19*	70.4	1.5	
	093401.9+551428.4B	22.9 ± 6.9	RAY	1.31 (fixed)	1.0 (fixed)		2.0	0.053	Extended

NOTE. — Column 1: Source name. Column 2: Source position given as CXOU JHHMMSS.S+DDMMSS.S. Column 3: Background-subtracted 0.5–8.0 keV counts accumulated over 60.1 ks (SBS 0335–052) and 40.8 ks (I Zw 18). Aperture photometry was performed using 95% encircled-energy radii for 1.5 keV for point sources, and individual background regions were selected adjacent to each source as noted in §2. The standard deviation for the source and background counts are computed following the method of Gehrels (1986) and are then combined following the “numerical method” described in §1.7.3 of Lyons (1991). Column 4: Spectral model used to fit data. POW indicates an absorbed power-law model, whereas RAY (VRAY) indicates an absorbed Raymond-Smith thermal plasma model (with variable O abundance) (Raymond & Smith 1977). Columns 5 and 6: Neutral hydrogen absorption column density (N_{H}) in units of 10^{21} cm^{-2} . Photon index (Γ) or thermal plasma temperature (kT in units of keV) as determined from the best-fit absorbed power-law or thermal plasma models to the ACIS spectra. Also listed are the 90% confidence errors calculated for one parameter of interest ($\Delta\chi^2 = 2.7$). Column 7: Goodness of fit/degree of freedom. For SBS 0335–052, fitting was performed with the χ -statistic, while for I Zw 18 the χ^2 statistic was used (denoted by “*”). Columns 8 and 9: Observed 0.5–10.0 keV fluxes in units of $10^{-15} \text{ erg cm}^{-2} \text{ s}^{-1}$ and absorption-corrected 0.5–10.0 keV luminosities in units of $10^{39} \text{ erg s}^{-1}$, assuming the best-fit model parameters given in Columns 5 and 6. Column 10: Comments.

the damped L_{α} profile in a *HST/GHRS* UV spectrum. They found $N_{\text{HI}} = (7.0 \pm 0.5) \times 10^{21} \text{ cm}^{-2}$. This is nearly 10 times larger than the peak HI column density of $7.4 \times 10^{20} \text{ cm}^{-2}$ which (Pustilnik et al. 2001) found in their *VLA* HI map of SBS 0335–052. This large difference can be understood as a beam-smearing effect in the *VLA* map. The synthesized *VLA* beam ($20''.5 \times 15''.0$) is considerably larger than the *GHRS* aperture ($2''.0 \times 2''.0$), and column densities in the direction of structures smaller than the *VLA* beam will be artificially diminished. Thus, for the X-ray point source associated with SBS 0335–052, the HI column density obtained from the spectrum through the small *GHRS* aperture is the appropriate one to use. No comparable *HST/GHRS* spectrum exists for SBS 0335–052W. The *VLA* map (Pustilnik et al. 2001) shows that the HI column density towards SBS 0335–052W to be 1.35 larger as compared to SBS 0335–052. For lack of better information, we have simply scaled the *GHRS* HI column density towards SBS 0335–052 by that factor to obtain the HI column density towards SBS 0335–052W. However, we should remember that, because of the large *VLA* beam, we do not know the exact value of $N(\text{HI})$ in the inner $2''$ of SBS 0335–052W, where the X-ray emission is located. For the HI column density towards I Zw 18, we have adopted the value $N_{\text{HI}} = (3.5 \pm 0.5) \times 10^{21} \text{ cm}^{-2}$ derived by (Kunth et al. 1994) in the same way as for SBS 0335–052, by fitting the wings of the damped L_{α} profile in a *HST/GHRS* spectrum of the NW component, obtained through a $2''.0 \times 2''.0$ aperture. This value is entirely consistent with the value of $2.1 \times 10^{21} \text{ cm}^{-2}$ derived by Vidal-Madjar (2000) from fitting the $\text{Ly}\beta$ absorption profile, with that of $(2.0 \pm 0.5) \times 10^{21} \text{ cm}^{-2}$ obtained by Lecavelier des Etangs et al. (2003) and that of $2.2^{+0.6}_{-0.5} \times 10^{21} \text{ cm}^{-2}$ obtained by Aloisi et al. (2003) by fitting the blue wing of the $\text{Ly}\beta$ line and the profiles of several other lines of the HI Lyman series. The last three determinations are based on *FUSE* spectra obtained through a $30''.0 \times 30''.0$ aperture. Brown et al. (2002) have obtained *STIS* data of I Zw

18 at the very high spatial resolution of $0''.5$. They discovered significant inhomogeneity in the HI gas, with a peak as high as $N_{\text{HI}} \sim 2 \times 10^{22} \text{ cm}^{-2}$. However, this is not the appropriate value to use here as this HI peak is associated with the SE component, while the X-ray source is associated with the NW component which (Kunth et al. 1994) observed. *VLA* HI maps of I Zw 18 have been obtained by van Zee et al. (1998). They also found a peak HI column density at the SE component of $\sim 3 \times 10^{21} \text{ cm}^{-2}$. Again, because the highest resolution map of van Zee et al. (1998) has a beam size of $5''.2 \times 4''.8$, beam smearing effects have decreased the real HI peak column density by a factor of nearly 10.

The ACIS spectra of the sources in SBS 0335–052, SBS 0335–052W, and I Zw 18 were fit with two types of models, absorbed thermal plasma models (*zwabs+raymond*; Raymond & Smith 1977) and absorbed power-law models (*zwabs+pow*). Given the limited counting statistics, we performed the spectral analysis using the unbinned, background-subtracted source spectra and the Cash statistic (Cash 1979), which is well suited to low-count sources (e.g., Nousek & Shue 1989). Note that we expect $\lesssim 2$ background counts in the source aperture, so spurious residuals from spatially varying background should be negligible. One limitation of the Cash statistic is that it does not provide a reliable quality-of-fit criterion (like the χ^2 statistic) to compare different models. Therefore, we established the quality of the spectral results via visual inspection using the binned spectrum. None of the sources have enough counts to constrain strongly both the column density and the temperature or photon index. In our spectral fits using a thermal plasma model, we have assumed an abundance of $Z = 0.025Z_{\odot}$ for SBS 0335–052, and $Z = 0.02Z_{\odot}$ for SBS 0335–052W and I Zw 18, in accordance with the abundances determined spectroscopically (see Izotov et al. 1999 for SBS 0335–052 and I Zw 18, and Lipovetsky et al. 1999 for SBS 0335–052W).

The spectrum of the point source in SBS 0335–052 has only

≈ 29 counts and is not strongly constrained by either the absorbed power-law or thermal plasma models when the column density N_{H} is left as a free parameter in the fit (see Table 1). If we fix N_{H} to the HI value of $7 \times 10^{21} \text{ cm}^2$ obtained from fitting the Ly α profile (Thuan & Izotov 1997), we find that the spectrum is moderately soft, with best-fit values of the photon index $\Gamma = 2.2_{-0.8}^{+0.6}$ ($\Gamma = \alpha + 1$, where α is the slope of the power-law fit) or $kT = 2.7_{-1.3}^{+16.6}$ keV. These values are consistent with those of black-hole X-ray binaries (e.g., $\Gamma \sim 1.7$ – 2.2 ; Foschini et al. 2002; Roberts et al. 2003), but are not consistent with a hot gas component heated by supernovae which has typically $kT < 1$ keV. The point source has an unabsorbed X-ray luminosity of $(2.8\text{--}3.5) \times 10^{39} \text{ erg s}^{-1}$. The spectrum and lack of variability do not provide further constraints on the nature of this source.

The spectrum of the brighter component point source (#1) in SBS 0335–052W is acceptably fit by both the absorbed power-law or thermal plasma models. The best fit parameters are $N_{\text{HI}} = (5.2_{-2.7}^{+3.3}) \times 10^{21} \text{ cm}^{-2}$, $\Gamma = 2.8_{-0.8}^{+0.9}$ and $N_{\text{HI}} = (3.1_{-1.9}^{+2.3}) \times 10^{21} \text{ cm}^{-2}$, $kT = 2.0_{-0.8}^{+2.2}$ keV, respectively (see Table 1). The N_{H} vs. Γ and N_{H} vs. kT confidence contours for SBS 0335–052W #1 are given in Figure 2, indicating the relative accuracy of the derived parameters. The soft intrinsic spectrum is similar to that of the point source in SBS 0335–052, and is not consistent with the typical hot gas component seen in other galaxies. The best fit values of N_{H} in both models are higher than the beam-diluted $N_{\text{HI}} = 1.0 \times 10^{21} \text{ cm}^{-2}$ obtained from the VLA HI map. However, they are lower than the value of $9.5 \times 10^{21} \text{ cm}^{-2}$ obtained from scaling the N_{HI} obtained from the fit of the damped Ly α profile in SBS 0335–052 by the ratio of radio HI column densities of 1.35 between SBS 0335–052 and SBS 0335–052W (Pustilnik et al. 2001). The point source in SBS 0335–052W has an unabsorbed X-ray luminosity in the range $(5.2\text{--}8.5) \times 10^{39} \text{ erg s}^{-1}$.

The spectrum of the fainter component point source (#2) in SBS 0335–052W is also acceptably fit by both the absorbed power-law or thermal plasma models. The best fit parameters are $N_{\text{H}} = 2.3(< 7.1) \times 10^{21} \text{ cm}^2$, $\Gamma = 1.9_{-0.8}^{+1.1}$ and $N_{\text{H}} = 1.3(< 3.0) \times 10^{21} \text{ cm}^2$, $kT = 5.4(> 1.9)$ keV, respectively (see Table 1). Although the column density is not well constrained, the upper limits are in good agreement with those from point source #1. The intrinsic spectrum of this source is the hardest of the three discussed so far, but it is still relatively soft. This point source has an unabsorbed X-ray luminosity in the range $(2.4\text{--}2.8) \times 10^{39} \text{ erg s}^{-1}$.

The spectrum of I Zw 18 has much better photon statistics than SBS 0335–052, so we grouped the X-ray spectra in 20-count bins and fit the data using χ^2 . The absorbed power-law model provides a slightly better fit to the continuum than the absorbed thermal plasma model, although both are formally acceptable. The best fit parameters are $N_{\text{H}} = (1.44_{-0.37}^{+0.38}) \times 10^{21} \text{ cm}^{-2}$, $\Gamma = 2.01_{-0.16}^{+0.14}$ and $N_{\text{H}} = (0.87_{-0.24}^{+0.27}) \times 10^{21} \text{ cm}^{-2}$, $kT = 4.06_{-1.19}^{+1.84}$ keV, respectively (see Table 1). Interestingly, we find large residuals below ≈ 1 keV, particularly around ≈ 0.65 keV, which is most likely caused by one or more emission lines. Bomans & Weis (2002) also found this line, accounting for about 3% of the total flux, which they attributed to the OVIII hydrogen-like emission line.

One way to account for this particular emission feature is an O enhancement in the X-ray gas. If we model the spectrum with an absorbed thermal plasma model, varying the O abundance but keeping all other elements fixed to $Z = 0.02Z_{\odot}$, we

find an improvement over the simple thermal model fit at the 99.99% confidence level (Figure 3). The best fit parameters are

$$N_{\text{H}} = (0.94_{-0.24}^{+0.35}) \times 10^{21} \text{ cm}^{-2}, \quad kT = 4.28_{-1.31}^{+2.25} \text{ keV}, \quad Z^{\text{O}} = 7.0_{-4.3}^{+12.2} Z_{\odot}^{\text{O}}, \quad (\text{see Table 1}).$$

To check for the possibility that α -elements other than O may also be contributing to the shape of the X-ray spectrum, we have also investigated a model where the abundances of the α -elements Ne, Si, S and Ar vary in concert with the O abundance, but in such a way that the α -element-to-oxygen abundance ratios Ne/O, Si/O, S/O and Ar/O remain constant, equal to the values derived by Izotov & Thuan (1999) for low-metallicity BCDs (see their Table 6). This model gives a worse fit to the X-ray spectrum. We conclude that the O abundance of the X-ray gas in the point source in I Zw 18 is likely to be enhanced by a factor of ~ 350 with respect to the O abundance determined for the HII region gas, while the other α -elements have abundances that are consistent with no enrichment with respect to the abundances in the HII region.

The point source in I Zw 18 has an unabsorbed X-ray luminosity between $1.3\text{--}1.5 \times 10^{39} \text{ erg s}^{-1}$, a factor of 2–4 times smaller than those found for SBS 0335–052. In addition to the point sources discussed previously, both SBS 0335–052 and I Zw 18 also show faint extended sources. The flux of the extended source in SBS 0335–052 is only about 10% of the 0.5–10 keV flux of the point source, and that of the one in I Zw 18 is only about 2.7% of the flux of the point source (Table 1). The physical nature of these extended sources will be discussed more in detail in the next section.

3. RESULTS AND DISCUSSION

Our main findings are the following:

1) X-ray emission is detected from both SBS 0335–052 and SBS 0335–052W, and from I Zw 18. The 0.5–10.0 keV luminosities of the three BCDs are in the range $1.3\text{--}8.5 \times 10^{39} \text{ erg s}^{-1}$. They are dominated by point sources, although at the distances of these objects and with the limited statistics, it is difficult to rule out emission from a collection of fainter point or compact extended sources. If these sources are single objects, their luminosities would place them in the range of the so-called ultraluminous X-ray sources (ULXs; e.g., Makishima et al. 2000)

The X-ray spectra of the point sources are well fitted by moderately soft power-laws, typical of X-ray emission from HMXBs or ULXs. The high X-ray luminosities of these sources could be the result of the lower metallicities of the BCDs studied here (if accretion is via stellar winds), or beaming (as is thought to occur in some ULXs; e.g., King et al. 2001). The mean luminosity of galactic HMXBs is $\sim 5 \times 10^{36} \text{ erg s}^{-1}$ (van Paradijs & McClintock 1995). The X-ray sources in SBS 0335–052, SBS 0335–052W and I Zw 18 are respectively about 600, 1300 and 300 times brighter. For comparison, the HMXBs in the Magellanic Clouds (the LMC and the SMC have respectively 1/3 and 1/8 of the Sun’s metallicity) are about 50 times brighter than their galactic counterparts (van Paradijs & McClintock 1995).

In the event of X-ray emission produced by accretion onto a compact object by a stellar wind, there are two main reasons which may explain the boosting of the X-ray luminosities of HMXBs in low-metallicity systems (van Paradijs & McClintock 1995). First, the X-ray heating of the gas as it falls toward a compact object depends strongly on the atomic number Z , since the photoelectric cross-section goes as Z^4 . Thus in low-metallicity systems, the X-ray heat-

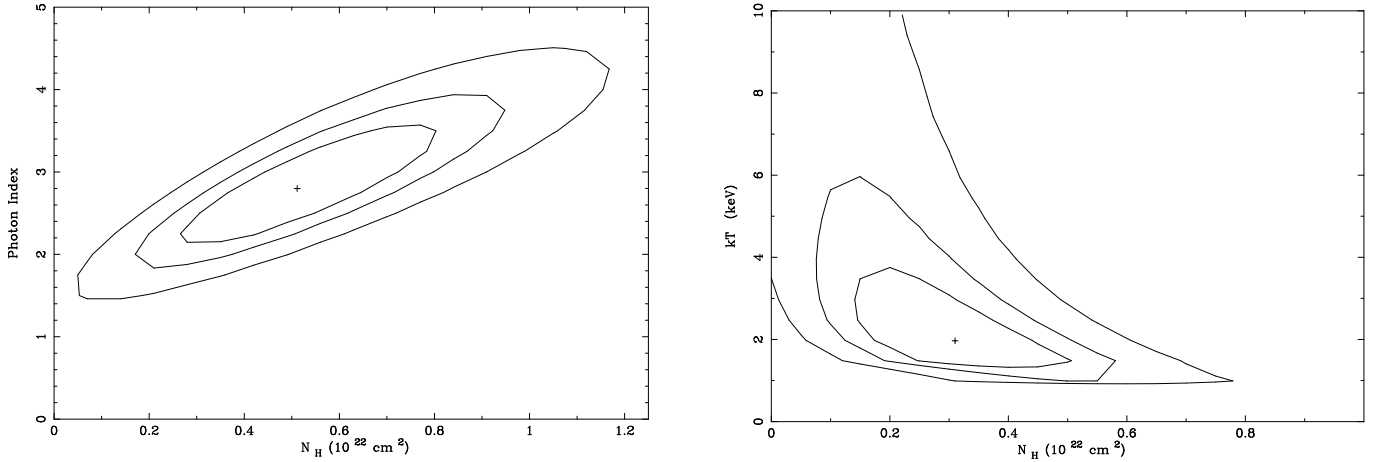


FIG. 2.— (Left) N_{H} vs. Γ and (Right) N_{H} vs. kT confidence contours for SBS 0335–052 West #1. Contours delineate the 66%, 95%, and 99% confidence regions.

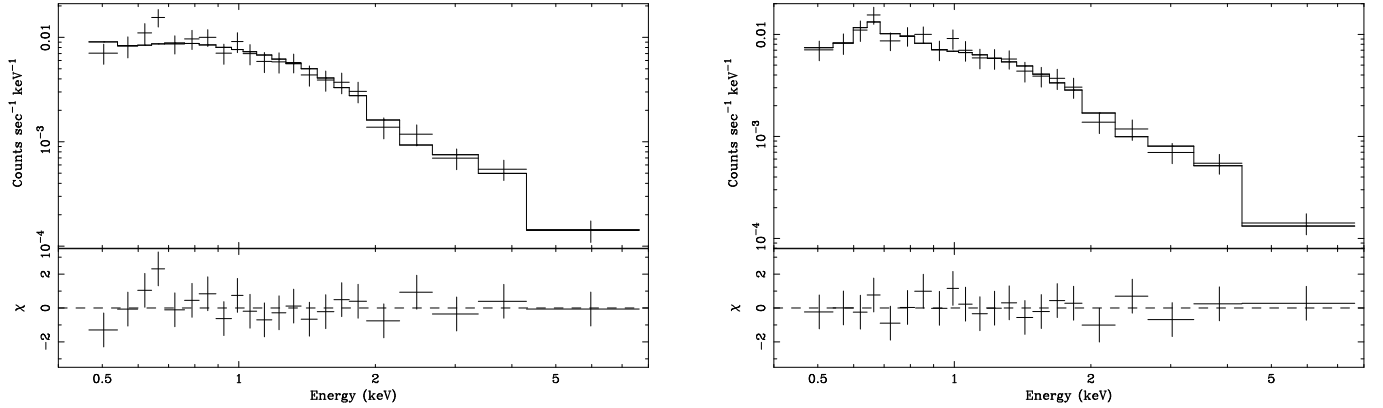


FIG. 3.— (Left) X-ray spectrum of I Zw 18 point source, modeled with an absorbed power-law of slope $\Gamma = 2.01$ and $N_{\text{H}} = 1.44 \times 10^{21} \text{ cm}^{-2}$. Note the large residuals around 0.65 keV suggesting the presence of an OVIII hydrogen-like emission line. (Right) Same spectrum, modeled with an absorbed thermal plasma of $kT = 4.28 \text{ keV}$, $N_{\text{H}} = 9.4 \times 10^{20} \text{ cm}^{-2}$, and an O abundance of $Z^{\text{O}} = 7.0Z_{\odot}$, which significantly improves the fit in the 0.65 keV region.

ing is less, resulting in a larger accretion rate because it is less impeded by heating. Second, the accretion rate dM/dt increases strongly as the stellar wind velocity v of an OB star as the orbit of the compact object decreases (dM/dt is proportional to v^{-4}). It is known that the terminal wind velocity in low-metallicity systems drops significantly. Thuan & Izotov (1997) have measured a terminal velocity of $\sim 500 \text{ km s}^{-1}$ for SBS 0335–052, as compared to 2000–4000 km s^{-1} for the Galaxy and the LMC, and 1200–1500 km s^{-1} for the SMC. Thus the high X-ray luminosities of the sources in the metal-deficient galaxies SBS 0335–052, SBS 0335–052W and I Zw 18 (i.e., $L_{\text{X}} > 10^{39} \text{ erg s}^{-1}$) do not necessarily require extreme black hole masses.

The X-ray luminosities found here are higher than the point-source luminosities observed in less metal-poor dwarf starburst dwarf galaxies such as NGC 3077 (Z_{\odot} , $L_{0.3-8.0 \text{ keV}} \approx 2-5 \times 10^{38}$, $\gtrsim 15\%$ from point sources; Ott, Martin, & Walter 2003), IC 10 ($Z_{\odot}/4$, $L_{0.3-8.0 \text{ keV}} \approx 2 \times 10^{38}$, $\gtrsim 95\%$ from a single point source; Bauer & Brandt 2003), NGC 4449 ($Z_{\odot}/4$, $L_{0.3-8.0 \text{ keV}} \approx 2 \times 10^{39}$, $\sim 60\%$ from point sources; Summers et al. 2003) and NGC 1569 ($Z_{\odot}/5$, $L_{0.3-6.0 \text{ keV}} \approx 1 \times 10^{39}$, $\sim 30\%$ from point sources; Martin, Kobulnicky, & Heckman 2002; Heike et al. 2003). They are comparable to the point source luminosity in Holmberg II ($Z_{\odot}/10$, $L_{0.1-10.0 \text{ keV}} \approx 1 \times 10^{40}$, $\gtrsim 75\%$ from a single point source; Miyaji, Lehmann, & Hasinger 2001).

Interestingly, Hunt et al. (2003b) have detected a non-thermal radio source associated with SSCs 1 and 2. Its flux density is $\sim 0.6 \text{ mJy}$ at 5 GHz, corresponding to a non-thermal radio luminosity of $\sim 2 \times 10^{20} \text{ W Hz}^{-1}$. Within the uncertainties in the X-ray and radio positions, the non-thermal radio source can be associated with the X-ray point source. However the nature of such a radio+X-ray emitting object is not clear. While its X-ray luminosity is similar to that expected from a microquasar associated with a medium-mass black hole, its radio luminosity is about a million times greater than that observed in such objects (Mirabel & Rodríguez 1999). It can also be that the X-ray and radio sources are physically distinct objects, although they are both associated with the massive starburst episode that gave birth to the SSCs.

We note also that the time scale for HMXB formation of 3–10 Myr after the onset of the starburst is consistent with the ages of 5 Myr or younger of SSCs 1 and 2 in SBS 0335–052 (Vanzi et al. 2000) and of ~ 3 Myr of the NW component in I Zw 18 (Hunt, Thuan, & Izotov 2003a).

2) In addition to the point source emission in SBS 0335–052 and I Zw 18, there appears also to be faint extended diffuse X-ray emission from hot gas, hints of which can be seen in the smoothed X-ray contours of Figure 1, particularly in I Zw 18. This emission, if truly diffuse, can be understood in both BCDs as produced by the hot gas filling the cavity of a superbubble carved out in the ISM of the BCD by stel-

lar winds and supernovae. Indeed, *HST* optical imaging by TIL shows a large superbubble cavity of radius ~ 380 pc in SBS 0335–052, northeast of SSC 3 (see their Figure 1), where the diffuse X-ray emission appears to lie. Using equations 2, 4 and 6 of Martin & Kennicutt (1995), the X-ray luminosity L_X of the superbubble is proportional to $R^{1.65}n^{0.66}T^{2.66}$, where R is the radius of the superbubble, n the ambient ISM density and T the gas temperature. Adopting $R = 380$ pc, $n = 12 \text{ cm}^{-3}$ and $T = 7.6 \times 10^6$ K, the predicted L_X is in good agreement with the observed diffuse X-ray luminosity of $6.4 \times 10^{38} \text{ ergs s}^{-1}$. As for I Zw 18, the diffuse X-ray emission lie between the NW and SE centers of star formation. *HST* optical imaging by Hunter & Thronson (1995) suggests the presence of a supernova cavity there of radius 120 pc (see their figure 3). With $R = 120$ pc, $n = 12 \text{ cm}^{-3}$ and $T = 6.0 \times 10^6$ K, L_X is equal to $5.3 \times 10^{37} \text{ ergs s}^{-1}$, again in good agreement with the observed diffuse X-ray luminosity in I Zw 18.

3) The spectrum of I Zw 18 shows a strong emission line at ~ 0.65 KeV, identified by Bomans & Weis (2002) to be a O VIII hydrogen-like line. The best spectral fit (Figure 3) gives an overabundance of oxygen by a factor of ~ 7 with respect to the Sun and of ~ 350 with respect to the other heavy elements. It is interesting that this line is so strong because *FUSE* observations of the HI interstellar gas in I Zw 18 (Aloisi et al. 2003; Lecavelier des Etangs et al. 2003) shows the ISM to be as or more metal-deficient than the HII gas, i.e. to be less than 2% of the solar metallicity. The presence of a sizable amount

of oxygen in the X-ray spectrum of the point source is most likely due to oxygen-enrichment by either a companion star (in the case of an X-ray binary) or undiluted supernova ejecta (in the case of hot gas).

Further progress in our understanding of the X-ray emission in SBS 0335–052, SBS 0335–052W and I Zw 18 will require substantially better photon statistics and higher spatial resolution. A long observation with *XMM-Newton*, or *Constellation-X/XEUS* in the future, would be able to provide better spectral and temporal constraints that might confirm the nature of the brightest point sources as true single compact objects or a collection of X-ray binaries and hot gas. However, such observations will not have the necessary spatial resolution for separating the different emission components seen by *Chandra*. Spatially resolving these objects with good sensitivity is beyond the capability of *Chandra* and must await the launch of *Generation-X* or a similar high-resolution X-ray observatory.

Putting our results in a cosmological context, we expect that the X-ray emission from high-redshift primordial galaxies to come mainly from very high luminosity HMXBs.

TXT acknowledges the partial financial support of CXC grant GO0-1149X. FEB thanks the hospitality of the Astronomy Department of the University of Virginia and acknowledges the financial support of CXC grant GO3-4112X and STScI grant HST-GO-09683.01A.

REFERENCES

- Abel, T., Bryan, G. L., & Norman, M. L. 2002, *Science*, 295, 93
Aloisi, A., Savaglio, S., Heckman, T.M., Hoopes, C.G., Leitherer, C., & Sembach, K.R. 2003, *ApJ*, 595, 760
Arnaud, K. A. 1996, in ASP Conf. Ser. 101, *Astronomical Data Analysis Software and Systems V*, ed. G. Jacoby, & J. Barnes (San Francisco: ASP), 17
Bauer, F. E., & Brandt, W. N. 2003, *ApJ*, in press
Bertin, E. & Arnouts, S. 1996, *A&AS*, 117, 393
Bomans, D.J., & Weis, K. 2002, in *The High Energy Universe at Sharp Focus: Chandra Science*, ed. E.M. Schlegel & S.D. Vrtilek (Provo: ASP), Vol. 262, 141
Bromm, V., Coppi, P. S., & Larson, R. B. 2002, *ApJ*, 564, 23
Brown, T.M, Heap, S.R., Hubeny, I., Lanz, T., & Linder, D. 2002, *ApJ*, 579, L75
Cash, W. 1979, *ApJ*, 228, 939
De Young, D. S. & Heckman, T. M. 1994, *ApJ*, 431, 598
Foschini, L. et al. 2002, *A&A*, 392, 817
Freeman, P. E., Kashyap, V., Rosner, R., & Lamb, D. Q. 2002, *ApJS*, 138, 185
Garmire, G. P., Bautz, M. W., Ford, P. G., Nousek, J. A., & Ricker, G. R. 2002, *Proc. SPIE*, 4851, 28
Gehrels, N. 1986, *ApJ*, 303, 336
Heike, K., Awaki, H., Misao, Y., Hayashida, K., & Weaver, K. A. 2003, *ApJ*, 591, L99
Hills, J. G. 1980, *ApJ*, 235, 986
Hunt, L.K, Dyer, K.K., Thuan, T.X., & Ulvestad, J. 2003b, *ApJ*, submitted
Hunt, L.K, Thuan, T.X., & Izotov, Y.I. 2003a, *ApJ*, 588, 281
Hunter, D.A., & Thronson, H.A., Jr. 1995, *ApJ*, 452, 238
Izotov, Y.I., Chaffee, F.H., Foltz, C.B., Green, R.F., Guseva, N.G., & Thuan, T.X. 1999, *ApJ*, 527, 757
Izotov, Y. I., Chaffee, F. H., & Schaerer, D. 2001, *A&A*, 378, L45
Izotov, Y. I., Lipovetsky, V. A., Chaffee, F. H., Foltz, C. B., Guseva, N. G., & Kniazev, A. Y. 1997, *ApJ*, 476, 698
Izotov, Y. I. & Thuan, T. X. 1999, *ApJ*, 511, 639
King, A. R., Davies, M. B., Ward, M. J., Fabbiano, G., & Elvis, M. 2001, *ApJ*, 552, L109
Kunth, D., Lequeux, J., Sargent, W.L.W., & Viallefond, F. 1994, *A&A*, 282, 709
Lecavelier des Etangs, Desert, J.-M., Kunth, D., Vidal-Madjar, A., Callejo, G., Ferlet, R., Hébrard, G., & Lebouteiller, V. 2003, *A&A*, in press
Leitherer, C. & Heckman, T. M. 1995, *ApJS*, 96, 9
Lipovetsky, V. A., Chaffee, F. H., Izotov, Y. I., Foltz, C. B., Kniazev, A. Y., & Hopp, U. 1999, *ApJ*, 519, 177
Lyons, L. 1991, *Data Analysis for Physical Science Students*. (Cambridge: Cambridge University Press)
Makishima, K. et al. 2000, *ApJ*, 535, 632
Martin, C.L., & Kennicutt, R.C., Jr. 1995, *ApJ*, 447, 171
Martin, C. L., Kobulnicky, H. A., & Heckman, T. M. 2002, *ApJ*, 574, 663
Mirabel, I.F., & Rodríguez, L.F. 1999, *ARAA*, 37, 409
Miyaji, T., Lehmann, I., & Hasinger, G. 2001, *AJ*, 121, 3041
Nousek, J. A. & Shue, D. R. 1989, *ApJ*, 342, 1207
Östlin, G. 2000, *ApJ*, 535, L99
Ott, J., Martin, C., & Walter, F. 2003, *ApJ*, 594, 776
Papaderos, P., Izotov, Y. I., Fricke, K. J., Thuan, T. X., & Guseva, N. G. 1998, *A&A*, 338, 43
Papaderos, P., Izotov, Y. I., Thuan, T. X., Noeske, K. G., Fricke, K. J., Guseva, N. G., & Green, R. F. 2002, *A&A*, 393, 461
Pustilnik, S. A., Brinks, E., Thuan, T. X., Lipovetsky, V. A., & Izotov, Y. I. 2001, *AJ*, 121, 1413
Raymond, J. C., & Smith, B. W. 1977, *ApJS*, 35, 419
Roberts, T. P., Goad, M. R., Ward, M. J., & Warwick, R. S. 2003, *MNRAS*, 342, 709
Steidel, C. C., Giavalisco, M., Pettini, M., Dickinson, M., & Adelberger, K. L. 1996, *ApJ*, 462, L17
Summers, L. K., Stevens, I. R., Strickland, D. K., & Heckman, T. M. 2003, *MNRAS*, 342, 690
Thuan, T. X. & Izotov, Y. I. 1997, *ApJ*, 489, 623
Thuan, T. X., Izotov, Y. I., & Lipovetsky, V. A. 1997, *ApJ*, 477, 661 (TIL)
Thuan, T.X., Sauvage, M., & Madden, S. 1999, *ApJ*, 516, 783
van Paradijs J. & McClintock J. E. 1995, in *X-ray Binaries*, eds. W. H. Lewin, J. van Paradijs, E. P. J. van den Heuvel (Cambridge Univ. Press, Cambridge), p. 58
van Zee, L., Westpfahl, D., Haynes, M., & Salzer, J. 1998, *AJ*, 115, 1000
Vanzi, L., Hunt, L.K., Thuan, T.X., & Izotov, Y.I. 2000, *A&A*, 363, 493
Vidal-Madjar et al. 2000, *ApJ*, 538, L77
Yoshii, Y. & Arimoto, N. 1987, *A&A*, 188, 13